

Energy & Environmental Science

Accepted Manuscript



This is an *Accepted Manuscript*, which has been through the Royal Society of Chemistry peer review process and has been accepted for publication.

Accepted Manuscripts are published online shortly after acceptance, before technical editing, formatting and proof reading. Using this free service, authors can make their results available to the community, in citable form, before we publish the edited article. We will replace this *Accepted Manuscript* with the edited and formatted *Advance Article* as soon as it is available.

You can find more information about *Accepted Manuscripts* in the [Information for Authors](#).

Please note that technical editing may introduce minor changes to the text and/or graphics, which may alter content. The journal's standard [Terms & Conditions](#) and the [Ethical guidelines](#) still apply. In no event shall the Royal Society of Chemistry be held responsible for any errors or omissions in this *Accepted Manuscript* or any consequences arising from the use of any information it contains.

Rate Limiting Interfacial Hole Transfer in Sb_2S_3 Solid-State Solar Cells

Jeffrey A. Christians¹, David T. Leighton Jr., and Prashant V. Kamat^{*1,2}

Department of Chemical and Biomolecular Engineering

University of Notre Dame

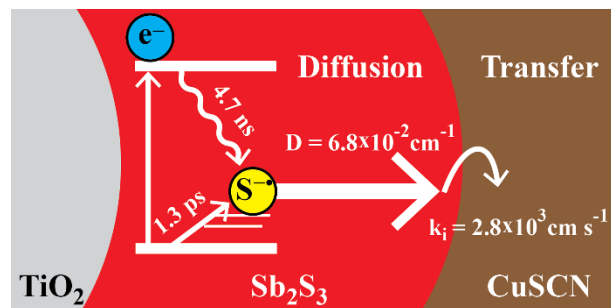
Notre Dame, Indiana 46556

*Corresponding author: pkamat@nd.edu

¹Radiation Laboratory, University of Notre Dame

²Department of Chemistry and Biochemistry, University of Notre Dame

TOC Entry



The hole diffusion coefficient and diffusion length in Sb_2S_3 is measured. Hole transfer from Sb_2S_3 to CuSCN is found to be predominately limited by transfer across the Sb_2S_3 – CuSCN interface.

Keywords

photovoltaics; solar cells; mobility; diffusion length; Sb_2S_3 ; CuSCN ; transient absorption spectroscopy; hole transfer; solid-state solar cells; extremely thin absorber solar cells

Abstract

Transfer of photogenerated holes from the absorber species to the p-type hole conductor is fundamental to the performance of solid-state sensitized solar cells. In this study, we comprehensively investigate hole diffusion in the Sb_2S_3 absorber and hole transfer across the Sb_2S_3 –CuSCN interface in the $\text{TiO}_2/\text{Sb}_2\text{S}_3/\text{CuSCN}$ system using femtosecond transient absorption spectroscopy, carrier diffusion modeling, and photovoltaic performance studies. Transfer of photogenerated holes from Sb_2S_3 to CuSCN is found to be dependent on Sb_2S_3 film thickness, a trend attributed to diffusion in the Sb_2S_3 absorber. However, modeling reveals that this process is not adequately described by diffusion limitations alone as has been assumed in similar systems. Therefore, both diffusion and transfer across the Sb_2S_3 –CuSCN interface are taken into account to describe the hole transfer dynamics. Modeling of diffusion and interfacial hole transfer effects reveal that interfacial hole transfer, not diffusion, is the predominate factor dictating the magnitude of the hole transfer rate, especially in thin (< 20 nm) Sb_2S_3 films. Lastly, the implications of these results are further explored by photovoltaic measurements using planar $\text{TiO}_2/\text{Sb}_2\text{S}_3/\text{CuSCN}$ solar cells to elucidate the role of hole transfer in photovoltaic performance.

Broader Context

Solid-state sensitized solar cells (SSCs) utilizing semiconductor absorbers overcome the issues of leakage and evaporation encountered in liquid-junction SSCs, and offer the potential for efficient, low cost photovoltaics. For widespread commercialization these solar cells require higher power conversion efficiency than is currently obtained with state-of-the-art devices. One critical component to this is the efficient extraction of photogenerated charges from the semiconductor absorber material. In this study, we decouple the two steps of hole transfer in the $\text{Sb}_2\text{S}_3/\text{CuSCN}$ system: diffusion of holes in the Sb_2S_3 absorber layer, and transfer of these holes across Sb_2S_3 –CuSCN interface. We find that interfacial transfer is the major limiting step in the thin (< 20 nm) Sb_2S_3 films used for high efficiency Sb_2S_3 photovoltaics. Decoupling of diffusion and interfacial transfer leads to a deeper understanding of the mechanism of hole transfer. This information has implications for the future design of semiconductor-based SSCs as it points to an important, often neglected interface, the absorber-hole conductor interface, which can play an important role in charge extraction.

Introduction

In the search for renewable carbon-neutral energy, sensitized solar cells (SSCs) have been widely studied as they offer the potential for inexpensive, highly efficient photovoltaics.^{1–4} These solar cells rely on the rapid transfer of photogenerated electrons and holes to an electron acceptor (typically TiO₂ or ZnO) and a hole acceptor (liquid redox couple or solid hole conductor) from the sensitizer (dye or semiconductor) to achieve efficient charge separation and extraction.^{4–6} Solid-state SSCs are of particular interest because of electrolyte leakage issues that have hindered the commercial prospects of liquid-junction SSCs.^{7,6,8} A wide variety of semiconductor sensitizers have been employed in solid-state SSCs including, CdSe,^{9–11} CdS,¹² In₂S₃,¹³ and Sb₂S₃.^{14–20} Of these sensitizer materials, Sb₂S₃ shows particular promise, providing reported efficiencies of 3.1%,¹⁸ 4.1%,¹⁹ 5.13%,²⁰ and 6.3%¹⁴ using spiro-OMeTAD, CuSCN, P3HT, and PCPDTBT-PCBM hole conductors, respectively. In addition, crystalline Sb₂S₃ has a band gap of 1.7–1.8 eV,²¹ allowing for absorption across the visible spectrum, and indicating that even higher efficiencies than those reported are achievable using Sb₂S₃.⁸

Because the charge separation process in SSCs is dictated by the relative rates of charge transfer and recombination, knowledge of these rates is of great importance for the design of higher efficiency devices.^{22,23} Toward this goal, we recently reported on the mechanism and rate of hole transfer between Sb₂S₃ and CuSCN.²⁴ This previous work elucidated the two-step nature of the hole transfer process by following the spectroscopic fingerprint of trapped holes (S^{•+} radical) in the Sb₂S₃. The present study expands on this previous work by investigating the diffusion of holes in the Sb₂S₃, and how this influences the hole transfer rate from Sb₂S₃ to CuSCN.

Minority carrier diffusion length, L_D , is an important parameter that aids in the determination of optimal solar cell architecture as it dictates the critical absorber dimension beyond which charges are no longer extracted efficiently.^{25–33} For example, low diffusion lengths seen in organic photovoltaics (typically $L_D < 20$ nm) necessitate the interpenetrating donor/acceptor network employed in bulk heterojunctions to optimize both charge extraction and light absorption.^{34,25,29} On the other hand, semiconductors, such as lead sulfide³¹ and lead halide perovskite,^{26,27} exhibit L_D from tens of nanometers to over a micron. This allows for the design of mesostructured extremely thin absorber,^{35,5,16} and planar heterojunction^{36,15} solar cells with efficient charge extraction.

For these reasons, the diffusion of S^{•+} in Sb₂S₃ is investigated by observing the decrease in the observed hole transfer rate to CuSCN as a function of increasing Sb₂S₃ thickness. Traditionally, diffusion in this type of system is modeled using an absorbing boundary condition which assumes infinitely fast transfer across the donor/acceptor interface (i.e. hole concentration goes to zero at this interface).^{27,26,34,33} However, herein we provide evidence that interfacial hole transfer also limits the hole transfer rate from

Sb_2S_3 to CuSCN. Therefore, a model is developed describing the balance between hole diffusion in the Sb_2S_3 layer and transfer across the Sb_2S_3 –CuSCN interface, and the results are compared to the standard diffusion model employing absorbing boundary conditions. The diffusion-transfer model developed provides a better picture of the hole dynamics in Sb_2S_3 than the traditional diffusion model. Also, taking interfacial transfer resistance into account provides a better estimate of the intrinsic properties of the Sb_2S_3 absorber. Conversely, the diffusion only model is able to accurately estimate such device parameters as the productive absorber thickness. Together, these two models provide complementary information that serves to elucidate the limitations and mechanism of hole transfer in Sb_2S_3 solar cells. Finally, these results are correlated to planar $\text{TiO}_2/\text{Sb}_2\text{S}_3/\text{CuSCN}$ photovoltaics, highlighting the importance of hole transfer to overall photovoltaic performance. These results offer a comprehensive understanding of the balance between hole diffusion and interfacial transfer and its effect on Sb_2S_3 photovoltaic performance.

Results and Discussion

Experimental Measurements of Sb_2S_3 –CuSCN Hole Transfer

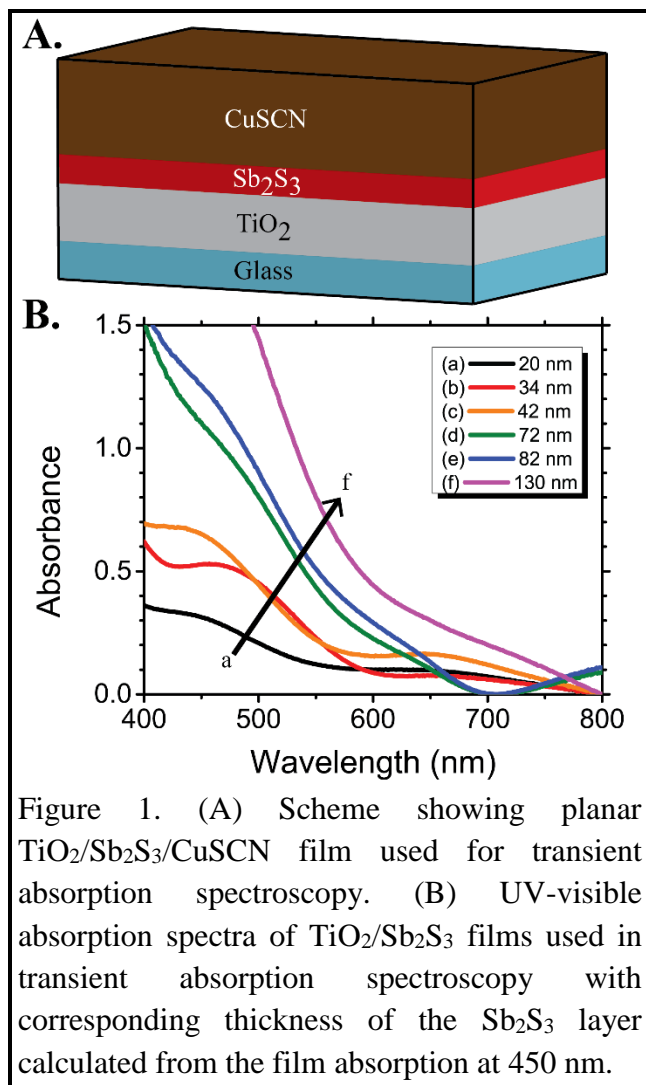


Figure 1. (A) Scheme showing planar $\text{TiO}_2/\text{Sb}_2\text{S}_3/\text{CuSCN}$ film used for transient absorption spectroscopy. (B) UV-visible absorption spectra of $\text{TiO}_2/\text{Sb}_2\text{S}_3$ films used in transient absorption spectroscopy with corresponding thickness of the Sb_2S_3 layer calculated from the film absorption at 450 nm.

To investigate the correlation between Sb_2S_3 film thickness and hole transfer, $\text{TiO}_2/\text{Sb}_2\text{S}_3$ and $\text{TiO}_2/\text{Sb}_2\text{S}_3/\text{CuSCN}$ films were prepared with varying Sb_2S_3 layer thickness. Sb_2S_3 films (20–130 nm) were deposited by chemical bath deposition on planar TiO_2 substrates. In contrast to the mesoporous TiO_2 substrates used in high efficiency Sb_2S_3 solar cells, planar TiO_2 substrates were employed to allow for precise control of Sb_2S_3 thickness (Figure 1A). The amorphous, as-deposited Sb_2S_3 was annealed under nitrogen to obtain crystalline Sb_2S_3 . As shown in Figure 1B, the thickness of the Sb_2S_3 layer was calculated from the absorption coefficient of the Sb_2S_3 films at 450 nm ($\alpha = 1.5 \times 10^5$).²⁴ Following characterization of $\text{TiO}_2/\text{Sb}_2\text{S}_3$ films, CuSCN was applied after KSCN treatment using a homemade automated deposition apparatus as described in the Experimental Methods.

Transient absorption spectroscopy is a useful tool to probe the recombination dynamics of semiconductor systems, and can be used to extract information about electron transfer reactions occurring in the system. Time-resolved difference absorption spectra of the Sb_2S_3 films described above were recorded over the time window of 0–1500 ps following a 387 nm laser pulse excitation. Transient absorption spectra of all films studied show three distinct features: an induced absorption peak at 560 nm attributed to the absorption of S^- arising from trapped holes in the Sb_2S_3 , and two photobleaching maxima at 460 nm and 650 nm attributed to the photobleaching of the first and second excitonic peaks in the steady-state absorption spectra. Absorption difference spectra of $\text{TiO}_2/\text{Sb}_2\text{S}_3$ and $\text{TiO}_2/\text{Sb}_2\text{S}_3/\text{CuSCN}$ films with a 34 nm Sb_2S_3 layer are shown in Figure 2 A and B, respectively. As detailed in our previous work,²⁴ hole transfer from Sb_2S_3 to CuSCN occurs *via* a two-step trap and transfer mechanism. Initially, photogenerated holes are trapped in Sb_2S_3 (reaction 1). These trapped holes are localized on one of the

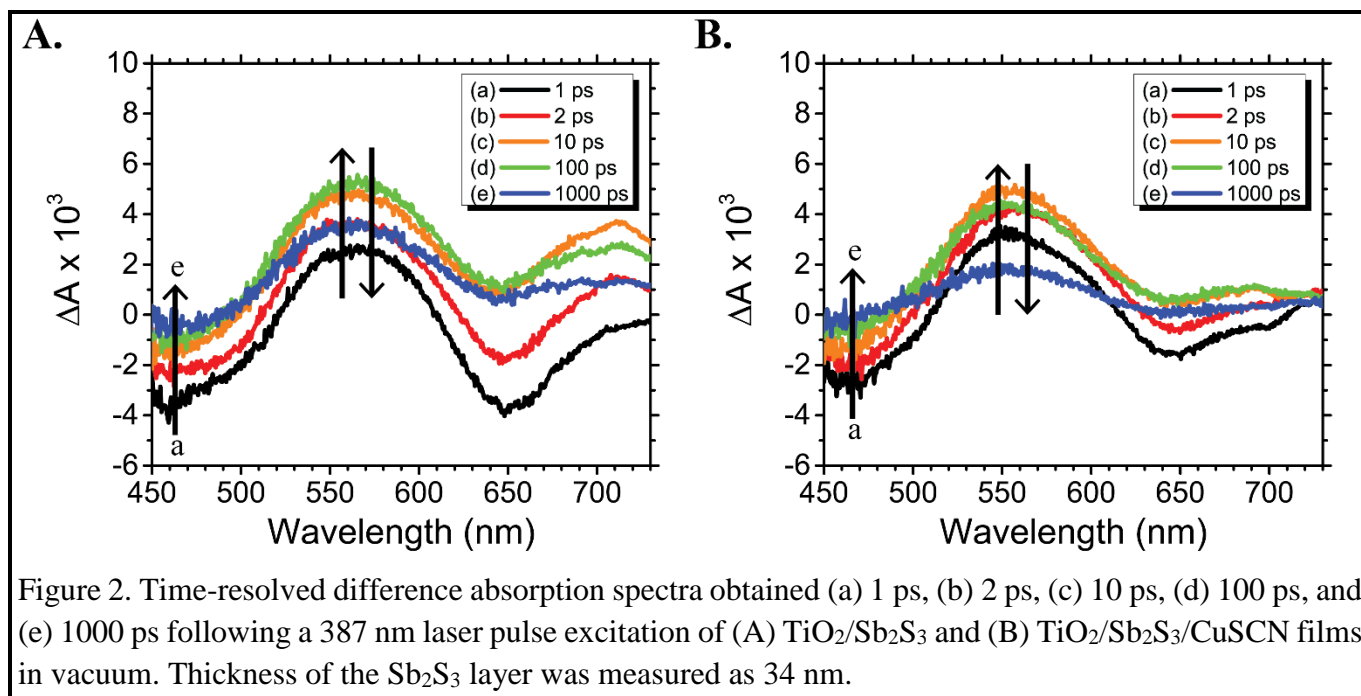


Figure 2. Time-resolved difference absorption spectra obtained (a) 1 ps, (b) 2 ps, (c) 10 ps, (d) 100 ps, and (e) 1000 ps following a 387 nm laser pulse excitation of (A) TiO₂/Sb₂S₃ and (B) TiO₂/Sb₂S₃/CuSCN films in vacuum. Thickness of the Sb₂S₃ layer was measured as 34 nm.

Sb₂S₃ sulfur atoms which gives rise to a spectral signal indicative of a S-radial anion (S⁻). This trapped hole is subsequently shown as S⁻ (or Sb₂S₂S⁻ when referring to it in the Sb₂S₃ crystal lattice). These trapped holes are then transferred from Sb₂S₃ to CuSCN (reaction 2) which results in the decay of the S⁻ induced absorption.



Based on previous studies of metal-chalcogenide semiconductor systems, the trapping of photogenerated charges is expected to take place on the surface of the Sb₂S₃ crystals.³⁷ The rate of hole trapping in Sb₂S₃ is independent of film thickness, as seen by the growth of the S⁻ absorption at 560 nm in Figure 3A. Hole trapping is also seen to be independent of the presence of CuSCN as shown in Figure 3B. This indicates that S⁻ formation does not occur primarily at the Sb₂S₃ surface or at the Sb₂S₃/CuSCN interface. Instead, this trapping may occur in the bulk crystallite through the breaking of the weak Sb–S bonds in the Sb₂S₃ lattice.^{38,24} Thus, it can be assumed that photogenerated holes are trapped as S⁻ at or near the point of generation in the Sb₂S₃ film, which implies that they must diffuse to the Sb₂S₃–CuSCN interface before transfer to CuSCN.

Hole transfer rates were calculated by comparing the decay of the S⁻ absorption in the presence and absence of CuSCN. Recently, O'Mahony et al. showed that an electron acceptor is not required for efficient hole extraction, and that charge separation may be initiated by hole extraction.²² Therefore, in the case of TiO₂/Sb₂S₃ films without CuSCN, we attribute the decay of trapped holes (*viz.* the S⁻ species) to non-radiative electron-hole recombination (reaction 3). The addition of CuSCN opens an additional

decay pathway, transfer of holes to CuSCN (reaction 2), which is expected to increase the rate of the $S^{\bullet-}$ decay.



Kinetic traces of the decay of the $S^{\bullet-}$ at 560 nm were assembled from the time-resolved transient absorption spectral data and modeled using a triexponential model (eq 4).

$$y = C[-e^{(-t/\tau_1)} + Ae^{(-t/\tau_2)} + (1 - A)e^{(-t/\tau_3)}] \quad (4)$$

These fits yielded an exponential saturation (τ_1), a short (τ_2) and long (τ_3) decay lifetime, a weighted coefficient (A) representing the contribution of the decay lifetimes to the overall transient signal decay, and the magnitude of the induced absorption signal (C). It is assumed that the transient kinetics of the varying thicknesses of Sb_2S_3 films are identical as all films studied are thick compared to the exciton Bohr radius of Sb_2S_3 .³⁹ Therefore, the kinetic lifetimes (τ_1 , τ_2 , and τ_3) and weighting coefficient (A) used were

determined from all TiO_2/Sb_2S_3 films simultaneously, while the signal magnitude (C) was allowed to vary between kinetic traces. This fitting was found to adequately describe the kinetics of the induced absorption signal for all TiO_2/Sb_2S_3 films studied. The largest discrepancy was seen for the 20 nm thick Sb_2S_3 film; however, the low transient absorption signal and potential residual absorptions complicates the fitting of this film. The exponential growth ($\tau_1 = 1.26$ ps) of the $S^{\bullet-}$ induced absorption is attributed to hole trapping (reaction 1). Subsequently, holes undergo two decay pathways: a fast process ($\tau_2 = 184$ ps) responsible for 20% of the decay, and a slow pathway ($\tau_3 = 4.7$ ns) responsible for 80% of the observed decay. The presence of a biexponential hole decay indicates that there are two distinct trapped hole species in the Sb_2S_3 , one short-lived and another long-lived species. Future work is needed to better understand and suppress the mechanism by which the short-lived holes recombine to further improve charge collection.

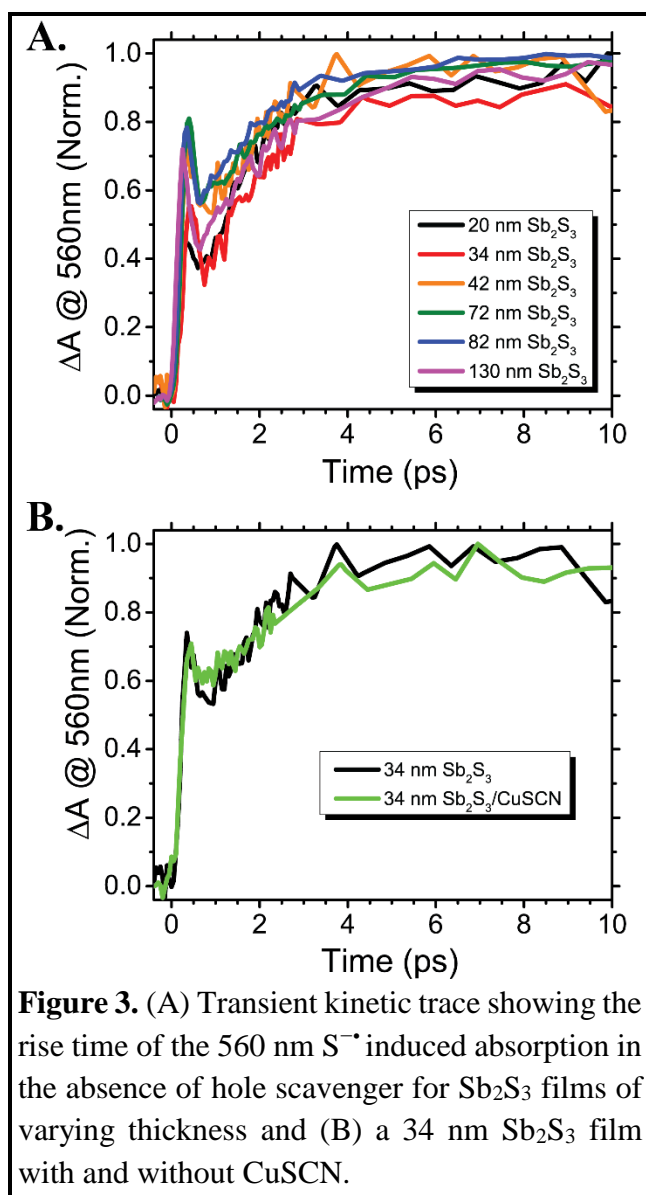


Figure 3. (A) Transient kinetic trace showing the rise time of the 560 nm $S^{\bullet-}$ induced absorption in the absence of hole scavenger for Sb_2S_3 films of varying thickness and (B) a 34 nm Sb_2S_3 film with and without CuSCN.

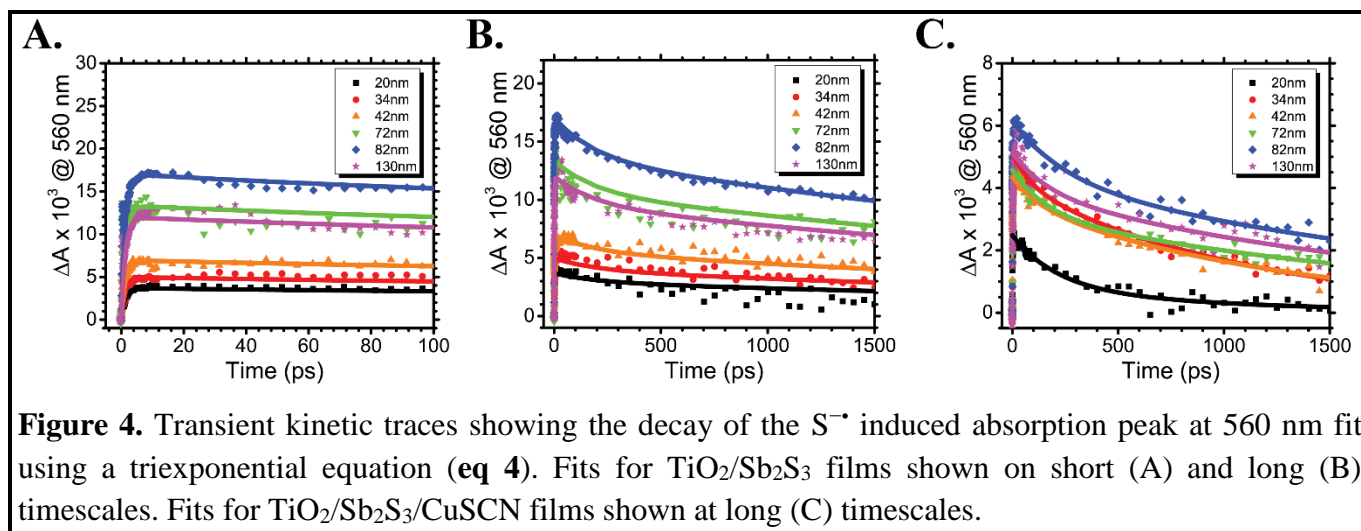


Figure 4. Transient kinetic traces showing the decay of the $S^{\bullet-}$ induced absorption peak at 560 nm fit using a triexponential equation (eq 4). Fits for $\text{TiO}_2/\text{Sb}_2\text{S}_3$ films shown on short (A) and long (B) timescales. Fits for $\text{TiO}_2/\text{Sb}_2\text{S}_3/\text{CuSCN}$ films shown at long (C) timescales.

Because hole trapping occurs at least two orders of magnitude faster than either recombination or transfer, and is not affected by CuSCN, kinetic modeling of $\text{TiO}_2/\text{Sb}_2\text{S}_3/\text{CuSCN}$ was done following the completion of hole trapping ($t > 6$ ps) for simplicity. Therefore, $\text{TiO}_2/\text{Sb}_2\text{S}_3/\text{CuSCN}$ kinetic traces were fit to a biexponential equation (eq 5).

$$y = C[Ae^{(-t/\tau_2)} + (1 - A)e^{(-t/\tau_3)}] \quad (5)$$

where C is the magnitude of the response, A is the weight and τ_2 is the lifetime of the short component of the decay, and τ_3 is the long component lifetime. Because the Sb_2S_3 films are different thicknesses, it is anticipated that the decay kinetics will vary between films due to differences in hole transfer, so all parameters were allowed to vary in order to best fit each transient kinetic trace.

The fitting parameters of all films studied are summarized in **Table 1**, and the transient kinetic data with fits are shown in **Figure 4A-C**. For $\text{TiO}_2/\text{Sb}_2\text{S}_3$ films, the short and long lifetimes of the $S^{\bullet-}$ absorption decay are attributed to non-radiative electron-hole recombination (**reaction 3**), while for $\text{TiO}_2/\text{Sb}_2\text{S}_3/\text{CuSCN}$ films it is attributed to both electron-hole recombination and hole transfer to CuSCN (**reaction 2 and 3**). To decouple recombination and hole transfer, it is assumed that there is no difference in the recombination dynamics in films with and without CuSCN. From this assumption, the estimated rate of hole transfer, k_{ht} , from Sb_2S_3 to CuSCN can be calculated from the average lifetime of the $S^{\bullet-}$ absorption by eq 6:

$$k_{ht} = 1/\langle\tau\rangle_{\text{Sb}_2\text{S}_3/\text{CuSCN}} - 1/\langle\tau\rangle_{\text{Sb}_2\text{S}_3} \quad (6)$$

where k_{ht} is the estimated hole transfer rate, and $\langle\tau\rangle_{\text{Sb}_2\text{S}_3/\text{CuSCN}}$ and $\langle\tau\rangle_{\text{Sb}_2\text{S}_3}$ are the average lifetimes of the decay in the presence and absence of CuSCN, respectively. Unlike the case without CuSCN where a single set of parameters described the dynamics of all Sb_2S_3 film thicknesses, we find that the presence of CuSCN requires A , τ_2 , and τ_3 to vary. As a result the estimated hole transfer rate, k_{ht} , is found, as shown in **Figure 5**, to be dependent on Sb_2S_3 film thickness. It is expected that the primary reason hole transfer

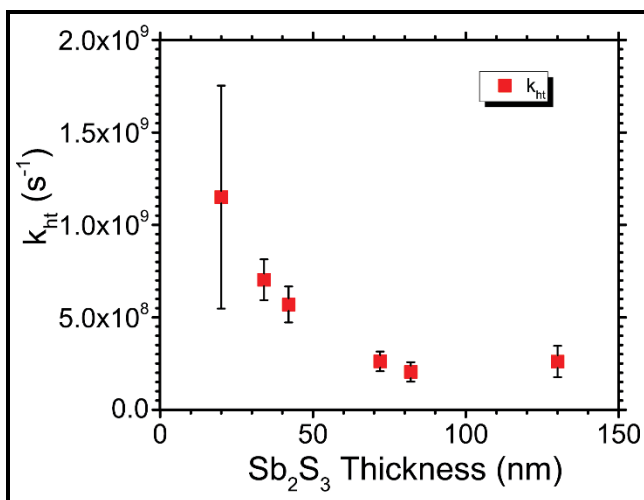
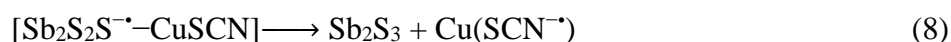
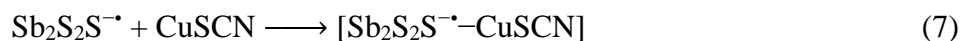


Figure 5. Trace showing how the estimated hole transfer rate calculated decreases with increasing Sb₂S₃ film thickness. Error bars represent the error in k_{ht} as calculated from the error of the fitting parameters as shown in Table 1.

rate decreases with increasing film thickness is the diffusion of photogenerated holes from their point of generation in the Sb₂S₃ film to the Sb₂S₃–CuSCN interface.

Taken as a whole, the proposed mechanism for hole transfer is as follows: (i) laser pulse excitation creates photogenerated holes in Sb₂S₃. (ii) Photogenerated holes are trapped in two distinct trap sites with approximately 20% of holes trapped in short-lived states and 80% in long-lived states. (iii) Short and long-lived holes recombine with exponential time constants estimated as 184 ± 45 ps and 4.7 ± 0.7 ns, respectively. (iv) In addition to

recombination, holes diffuse *via* a random walk through the Sb₂S₃ film to the Sb₂S₃–CuSCN interface (**reaction 7**) where, (v) they then can be transferred across this interface into CuSCN (**reaction 8**).



While it is traditionally assumed that the rate of interfacial transfer (**reaction 8**) is much faster than hole diffusion (**reaction 7**), this is not necessarily the case. Therefore, the contribution by each of these processes was studied in detail. To do this we employ two distinct hole transfer models: one which includes both diffusion and interfacial hole transfer, and a second that considers only hole diffusion in the Sb₂S₃ sensitizer. In the following sections the results of these two models are compared in detail.

Table 1. Summary of the results of fitting of induced absorption decay at 560 nm.

Sample ^a	τ_1 (ps)	A	τ_2 (ps)	τ_3 (ps)	$\langle\tau\rangle$ (ps) ^b	k_{ht} ($\times 10^8$ s ⁻¹)
TiO ₂ /Sb ₂ S ₃ (20 - 130 nm)	1.26 \pm 0.02	20 \pm 2.7%	184 \pm 45	4680 \pm 700	4630 \pm 700	--
TiO ₂ /Sb ₂ S ₃ (20 nm)/CuSCN	--	66 \pm 27%	210 \pm 80	960 \pm 670	730 \pm 370	11.5 \pm 6.0
TiO ₂ /Sb ₂ S ₃ (34 nm)/CuSCN	--	18 \pm 2.8%	90 \pm 24	1110 \pm 56	1090 \pm 50	7.0 \pm 1.1
TiO ₂ /Sb ₂ S ₃ (42 nm)/CuSCN	--	19 \pm 4.8%	130 \pm 51	1300 \pm 120	1280 \pm 103	5.7 \pm 1.0
TiO ₂ /Sb ₂ S ₃ (72 nm)/CuSCN	--	31 \pm 4.5%	160 \pm 38	2170 \pm 310	2100 \pm 290	2.6 \pm 0.5
TiO ₂ /Sb ₂ S ₃ (82 nm)/CuSCN	--	29 \pm 7.4%	240 \pm 77	2480 \pm 550	2390 \pm 500	2.0 \pm 0.5
TiO ₂ /Sb ₂ S ₃ (130 nm)/CuSCN	--	25 \pm 11%	170 \pm 110	2160 \pm 660	2100 \pm 600	2.6 \pm 0.8

^aThickness of the Sb₂S₃ film as estimated by UV-visible absorption is shown in parenthesis

^bAverage lifetime $\langle\tau\rangle$ is calculated by the equation:⁴⁰ $\langle\tau\rangle = (A\tau_2^2 + (1 - A)\tau_3^2) / (A\tau_2 + (1 - A)\tau_3)$

Modeling Diffusion and Interfacial Transfer

Initially, we consider the case where both hole diffusion in Sb₂S₃ and hole transfer across the Sb₂S₃–CuSCN interface contribute to the observed hole transfer dynamics. Hole diffusion and interfacial transfer were modeled by the idealized system shown in **Figure 6**.^{41,33,42} It was assumed that the diffusion of holes is described by a one-dimensional random walk and they are removed from the Sb₂S₃ layer by either transfer to CuSCN, or electron-hole recombination. Recombination is assumed to act homogeneously throughout the Sb₂S₃ film and independently from diffusion and transfer. As previously

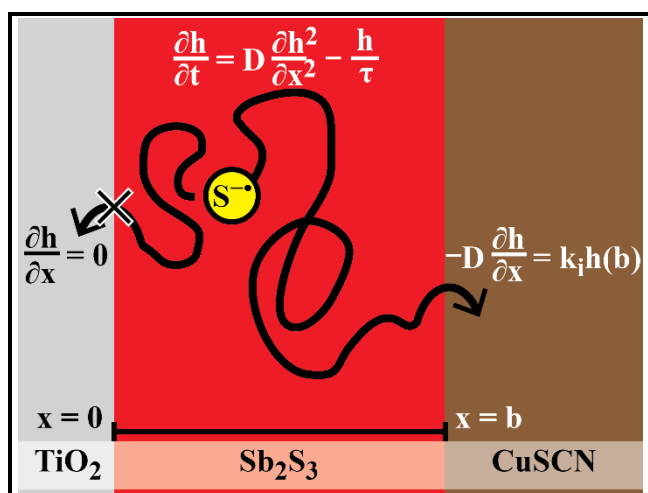


Figure 6. (A) Scheme showing the TiO₂/Sb₂S₃/CuSCN system modeled using Fick's second law of diffusion with appropriate boundary conditions.

discussed, there are two distinct hole species in the Sb₂S₃, one short-lived (h_s) and another long-lived (h_l). The short-lived holes make up a small proportion of the total trapped holes (20%), and decay rapidly by recombination. This means that these do not contribute significantly to the overall transfer process, so the results of the subsequent model are primarily influenced by long-lived holes. Therefore, the problem is simplified by assuming that there is no difference between h_s and h_l other than recombination rate. As previously, kinetic modeling was simplified by only looking at the decay following completion of hole trapping ($t > 6$ ps).

From these assumptions, the concentration of holes in Sb_2S_3 in the $\text{Sb}_2\text{S}_3/\text{CuSCN}$ films can be described as the linear combination of the contributions of short-lived and long-lived holes, ($h = h_s + h_l$) where each species can be described by a modified Fick's second law of diffusion as shown for h_l in **eq 9**.

$$\frac{\partial h_l}{\partial t} = D \frac{\partial^2 h_l}{\partial x^2} - h_l/\tau_3 \quad (9)$$

where h_l is the concentration of the long-lived holes in Sb_2S_3 in the $\text{TiO}_2/\text{Sb}_2\text{S}_3/\text{CuSCN}$ films, D is the effective hole diffusion coefficient, and τ_3 is the lifetime derived from the fitting of the kinetics of $\text{TiO}_2/\text{Sb}_2\text{S}_3$ films in the absence of CuSCN , shown in **Table 1**. Since it is assumed that short-lived and long-lived holes only differ in their respective lifetime, we will only develop the solution for h_l in detail. As an initial condition, we assume trapped holes are distributed exponentially throughout the Sb_2S_3 film (**eq 10**), where α is the absorption coefficient at the 387 nm excitation wavelength. For boundary conditions, we assume that there is no hole transfer between the Sb_2S_3 and TiO_2 (**eq 11**), and that the flux of holes across the Sb_2S_3 - CuSCN heterojunction is pseudo first order with respect to the concentration of holes at the interface (**eq 12**), where k_i is the proportionality constant or interfacial hole transfer coefficient.

$$h_l|_{t=0} = (1 - A)h_0 e^{-\alpha x}; 0 \leq x \leq b \quad (10)$$

$$\frac{\partial h_l}{\partial x}|_{x=0} = 0; t > 0 \quad (11)$$

$$-D \frac{\partial h_l}{\partial x}|_{x=b} = k_i h_l|_{x=b}; t > 0 \quad (12)$$

Solving this problem for the concentration of long-lived holes yields the infinite sum shown in **eq 13**, where σ_n is n^{th} eigenvalue of the eigenfunction shown in **eq 14**, and the constants B_n are derived from the initial condition. The solution for short-lived holes, h_s , is analogous to this solution as described in detail in the **Supporting Information**.

$$h_l = (1 - A)e^{-t/\tau_3} \sum_{n=1}^{\infty} B_n e^{-\frac{\sigma_n^2 D}{b^2} t} \cos(\sigma_n x/b) \quad (13)$$

$$\frac{k_i b}{D} = \sigma_n \tan(\sigma_n) \quad (14)$$

Next, in order to fit the experimental transient absorption data, the predicted transient absorption response, s , was obtained by integrating the sum of the concentration of short-lived and long-lived holes over the film thickness (**eq 15**). This calculated transient absorption signal (**eq 16**) is used to model the experimental transient kinetic traces to determine the values of k_i and D , and takes into account the contributions of both trapped hole species.

$$s = \int_0^b (h_s + h_l) dx \quad (15)$$

$$s = [Ae^{-t/\tau_2} + (1 - A)e^{-t/\tau_3}] \sum_{n=1}^{\infty} B_n \frac{\sin(\sigma_n)}{\sigma_n} e^{-\frac{\sigma_n^2 D}{b^2} t} \quad (16)$$

The parameters A , τ_2 , and τ_3 are no longer adjustable fitting constants, but rather taken as the fixed values derived from fitting of the TiO₂/Sb₂S₃ films in the absence of CuSCN. The predicted hole transfer rate, k_{model} , is calculated from the hole transfer lifetime of the modeled transient absorption decay, $b^2/\sigma_n^2 D$, and the leading coefficients by eq 17.

$$k_{model} = \left[\sum B_n \frac{\sin(\sigma_n)}{\sigma_n} \left(\frac{b^2}{\sigma_n^2 D} \right)^2 / \sum B_n \frac{\sin(\sigma_n)}{\sigma_n} \left(\frac{b^2}{\sigma_n^2 D} \right) \right]^{-1} \quad (17)$$

A full derivation of these solutions, including assumptions, is supplied in the **Supporting Information**. Eq 16 was approximated by the first five terms of the infinite sum ($n = 1-5$), and the model was fit to the transient kinetic decay of TiO₂/Sb₂S₃/CuSCN films (**Figure 7A**) to yield estimates for D and k_i . From these values, k_{model} was calculated by eq 17 as shown in **Figure 7B**. An estimate of the random

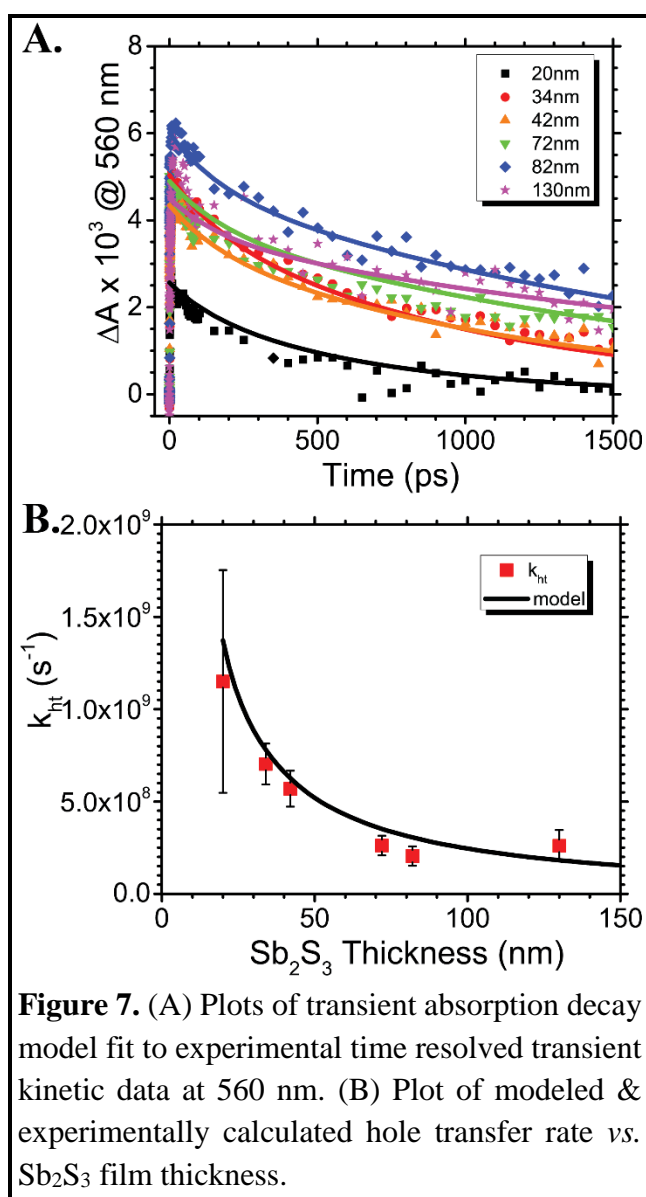


Figure 7. (A) Plots of transient absorption decay model fit to experimental time resolved transient kinetic data at 560 nm. (B) Plot of modeled & experimentally calculated hole transfer rate vs. Sb₂S₃ film thickness.

error in the calculated parameters was achieved via undersampling of the data set. From this model, the diffusion coefficient of trapped holes in Sb₂S₃ was estimated as $D = 6.8 \pm 4.7 \times 10^{-2} \text{ cm}^2 \text{ s}^{-1}$, and the interfacial hole transfer coefficient was estimated as $k_i = 2.8 \pm 0.2 \times 10^3 \text{ cm s}^{-1}$. From the calculated diffusion coefficient the mobility of the trapped holes in Sb₂S₃ was calculated to be $2.6 \pm 1.9 \text{ cm}^2 \text{ V}^{-1} \text{ s}^{-1}$ using the Einstein relation shown in eq 18.

$$D = \frac{k_B T \mu}{q} \quad (18)$$

where k_B is the Boltzmann constant, T is the temperature, μ is the carrier mobility, and q is the elementary charge. This hole mobility is $\sim 25\%$ of the reported electron mobility in Sb₂S₃ films determined using Hall effect measurements.⁴³ The high mobility in Sb₂S₃ of both electrons and holes is likely a major contributing factor to the high efficiency of Sb₂S₃ photovoltaics.

Another important parameter for thin film photovoltaic applications is the minority carrier diffusion length, L_D , given by eq 19.³⁴

$$L_D = \sqrt{D\tau} \quad (19)$$

where D is the diffusion coefficient, and τ is the hole lifetime. The average lifetime of the S^- species was determined to be 4.6 ns, as shown in **Table 1**. From this lifetime, L_D was calculated to be 180 ± 60 nm. Because diffusion and interfacial hole transfer are decoupled in this analysis, L_D provides information on carrier diffusion in Sb_2S_3 , but overestimates the productive thickness of Sb_2S_3 in a photovoltaic device. This overestimation is because interfacial transfer limitations decrease the Sb_2S_3 thickness for efficient charge extraction below the diffusion length.

An important parameter obtained from this model is the dimensionless parameter λ , shown in **eq 20**.

$$\lambda = \frac{k_i b}{D} \quad (20)$$

This parameter, referred to as the hole transfer Biot number, is analogous to the Biot number in mass and heat transfer.^{44,45} The hole transfer Biot number is the ratio of transfer at the Sb_2S_3 –CuSCN interface to diffusion in the Sb_2S_3 . Therefore, the value of λ can provide valuable information as to the limiting mechanism in overall hole transfer. If $\lambda \gg 1$, hole diffusion in the Sb_2S_3 film (**reaction 7**) is much slower than interfacial transfer (**reaction 8**), meaning that the overall hole transfer kinetics are primarily limited by diffusion. On the other hand, for $\lambda \ll 1$, diffusion is much faster than interfacial transfer, and hole transfer kinetics are limited by transfer across the Sb_2S_3 –CuSCN interface. Using the values for k_i and D obtained from the model, λ is calculated as $\lambda = 0.10 \pm 0.01$ for 20 nm Sb_2S_3 films and $\lambda = 0.64 \pm 0.05$ for 130 nm Sb_2S_3 films. As $\lambda < 1$, we find that interfacial transfer plays the major role in dictating the magnitude of the hole transfer rate, although diffusion effects become increasingly important as Sb_2S_3 film thickness increases. However, diffusion only becomes the *predominant* factor in determining hole transport kinetics as film thickness increases beyond 240 nm ($\lambda \approx 1$).

Modeling Diffusion Alone

The previous analysis suggests that interfacial transfer is an important factor to consider in the Sb_2S_3 /CuSCN system. However, in most models of this type, interfacial hole transfer is assumed to be very fast compared to diffusion.^{26,27,33,34,41} Therefore, it is of importance to confirm that the previous model is accurate by employing the simplified diffusion-only model. Instead of describing interfacial charge transfer as a pseudo first order process (**eq 12**), the assumption of infinitely fast interfacial transfer defines the concentration of holes at the interface to be zero at all time, t (**eq 21**), analogous to letting $k_i \rightarrow \infty$.

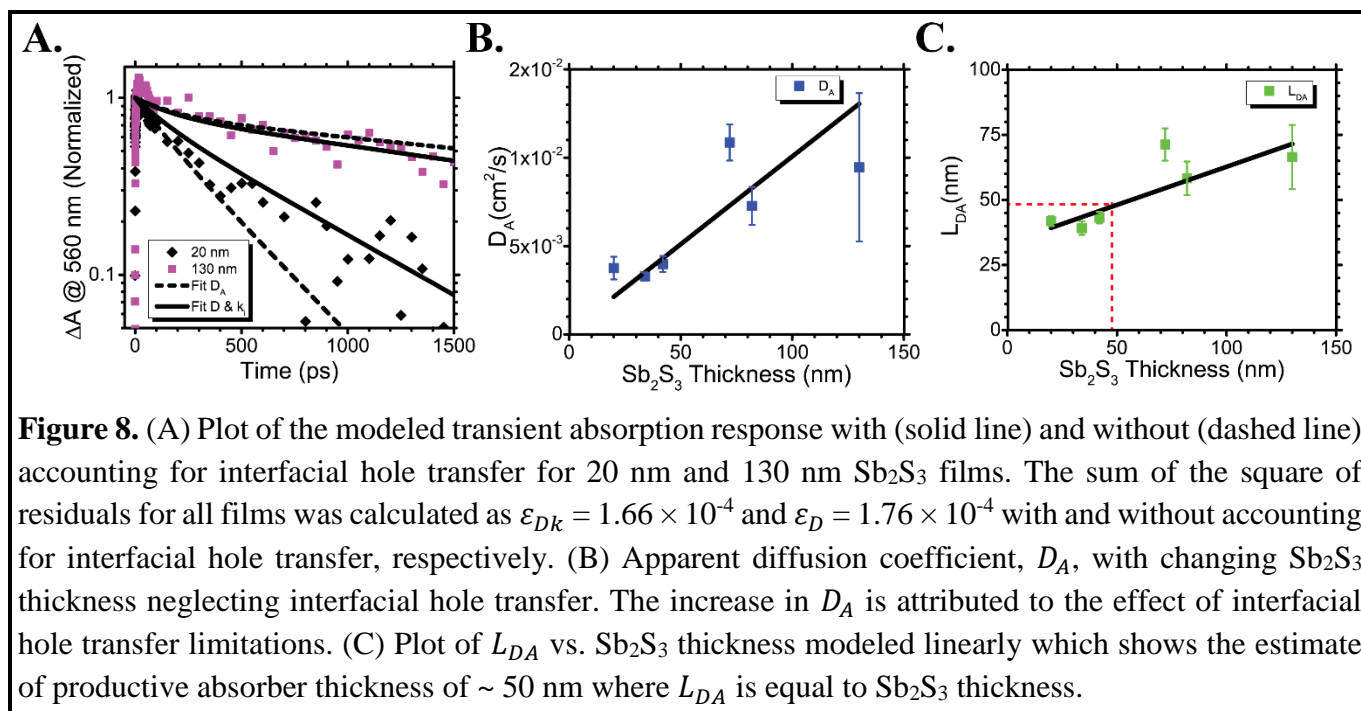
$$h|_{x=b} = 0; t > 0 \quad (21)$$

By neglecting the interfacial charge transfer and assigning all contributions to the overall hole transfer kinetics to diffusion, this model provide a lower bound estimate of the diffusion coefficient^{34,46,27} that is

only accurate in systems where diffusion is very slow compared to interfacial charge transfer (ie. $\lambda \gg 1$). This assumption breaks down when the overall transfer kinetics are significantly influenced by interfacial transfer. This more common model makes a very different assumption of the dynamics of hole transfer than the previously discussed interfacial transfer model. Because of this discrepancy (*viz.* slow interfacial transfer *vs.* infinitely fast interfacial transfer), the results of these two models were compared in detail. This is critical in determining if the data can be adequately explained by this simpler model, or if interfacial hole transfer really does play a major role as asserted.

This new diffusion model was solved analytically as before (**eq 9**) using the absorbing boundary condition (**eq 21**) in place of pseudo first order interfacial transfer (**eq 12**). The solution to this problem is obtained by taking the limit as $k_i \rightarrow \infty$ of **eq 16**. This new model was then used to fit the time-resolved absorbance data for the $\text{Sb}_2\text{S}_3/\text{CuSCN}$ films to obtain an apparent diffusion coefficient, D_A . The apparent diffusion coefficient of holes in Sb_2S_3 is estimated as $D_A = 4.3 \pm 0.3 \times 10^{-3} \text{ cm}^2 \text{ s}^{-1}$ when modeling all films simultaneously. This is an order of magnitude lower than the effective diffusion coefficient calculated when taking interfacial transfer into account using the constant flux boundary condition (**eq 12**). The quality of the fits from the two models were then compared at the two extreme film thicknesses, 20 nm and 130 nm, where interfacial processes have the most and least contribution, respectively (**Figure 8A**). It is seen that when a single apparent diffusion coefficient is used to describe the dynamics of all films at once (dashed lines), the absorbing boundary condition model does not capture the hole transfer dynamics as accurately at these extremes as the interfacial transfer model. While the diffusion-transfer model does provide a better fit, this alone does not provide conclusive evidence for interfacial hole transfer being a major factor in this system.

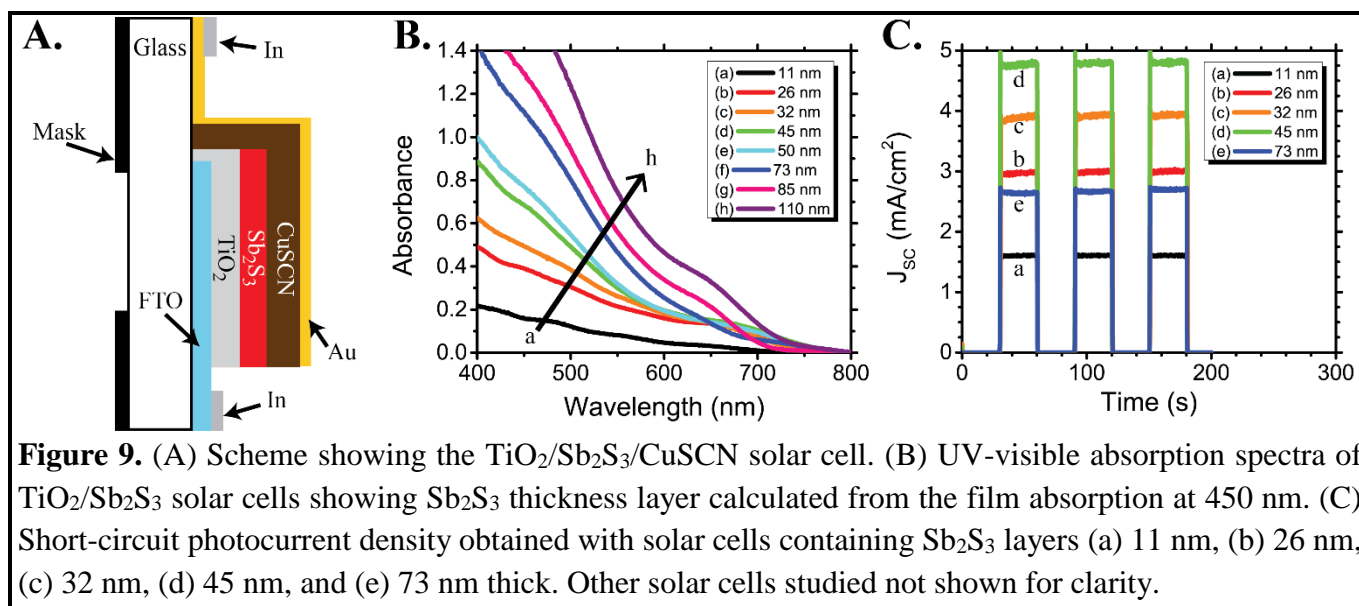
To further confirm the role of interfacial hole transfer, the apparent diffusion constant was calculated for each individual $\text{Sb}_2\text{S}_3/\text{CuSCN}$ film. If interfacial transfer is not a limiting factor, as assumed in this model, D_A should be constant. In contrast, as shown in **Figure 8B**, we observe that D_A increases with increasing film thickness. This behavior can be explained because interfacial transfer plays a more dominant role in decreasing hole transfer kinetics in thin films than in thick films. Together with the improved fit obtained using the diffusion-transfer model, the increase of D_A with Sb_2S_3 thickness clearly demonstrates the important role interfacial hole transfer plays in the $\text{Sb}_2\text{S}_3/\text{CuSCN}$ system. This confirms the validity of the results obtained from the previous diffusion-transfer model.



A comparison of the diffusion-transfer and diffusion-only models provides strong evidence that interfacial transfer limits the observed hole transfer dynamics. Nevertheless, analysis using absorbing boundary conditions can provide a useful estimate of the productive absorber thickness through the calculation of the apparent diffusion length, L_{DA} , as shown in **Figure 8C**. By neglecting interfacial hole transfer limitations in this model, L_{DA} combines the contributions of diffusion, interfacial transfer, and recombination into a single device specific parameter. Therefore, the productive absorber thickness was calculated by fitting the change of L_{DA} with thickness linearly and determining the point at which L_{DA} is equal to Sb_2S_3 thickness. Using this method, the productive absorber thickness was estimated as ~ 50 nm. This is not a rigorous calculation, but gives an estimate of the maximum Sb_2S_3 thickness that should be employed in a photovoltaic device to balance charge extraction and light absorption. This is significantly lower than the carrier diffusion length, $L_D = 180 \pm 60$ nm, because of interfacial hole transfer limitations.

Photovoltaic Performance

As seen both from transient absorption kinetics data and a modeling of the hole transfer process, thicker Sb_2S_3 films exhibit slower hole transfer due to charge carrier diffusion. However, it is not clear that this slower hole transfer will be detrimental to actual solar cell performance as device parameters are governed by a wide array of competing processes.^{47,48} Therefore, to explore the significance of this observation with respect to Sb_2S_3 photovoltaics, $\text{TiO}_2/\text{Sb}_2\text{S}_3/\text{CuSCN}$ solar cells were constructed as shown in **Figure 9A** with Sb_2S_3 films of varying thickness on planar nonporous TiO_2 substrates. UV-visible absorption spectra of the solar cells are shown in **Figure 9B** before CuSCN deposition. The short-circuit



current density (J_{SC}) of these solar cells measured under 100 mW cm^{-2} AM 1.5G simulated solar irradiation is presented in **Figure 9C**. J_{SC} increases initially with increasing Sb₂S₃ thickness due to increased light absorption. On the other hand, as the thickness of the Sb₂S₃ layer increases further, the kinetics of hole transfer are decreased by hole diffusion which increases electron-hole recombination, and consequently J_{SC} begins to decrease.

The photocurrent maximum was observed for the device with a 45 nm Sb₂S₃ film which correlates very well with the estimate of the productive absorber thickness of $\sim 50 \text{ nm}$, as calculated from L_{DA} . This agreement further establishes the power of diffusion analysis with absorbing boundary conditions for providing an estimation of the maximum critical absorber dimension in a photovoltaic device. In comparison, L_D is almost four times this value because it is an estimation of diffusion only, so it does not capture the interfacial hole transfer limitations which serve to decrease the productive absorber thickness below the diffusion limited value.

To further establish the link between photocurrent and hole transfer kinetics, we conducted external quantum efficiency (EQE) measurements shown in **Figure 10A**. From these measurements, the internal quantum efficiency (IQE) was calculated based on **eq 22** to correct for solar cell absorbance.

$$IQE = EQE / LHE \quad (22)$$

where LHE is the light harvesting efficiency or the percent of incident light absorbed by the solar cell. IQE provides a measurement of the efficiency with which absorbed photons are converted to photocurrent. The average IQE from 450 – 550 nm was compared to the hole transfer efficiency (HTE), shown in **Figure 10B**. HTE is calculated from the hole transfer kinetic data *via* **eq 23**.

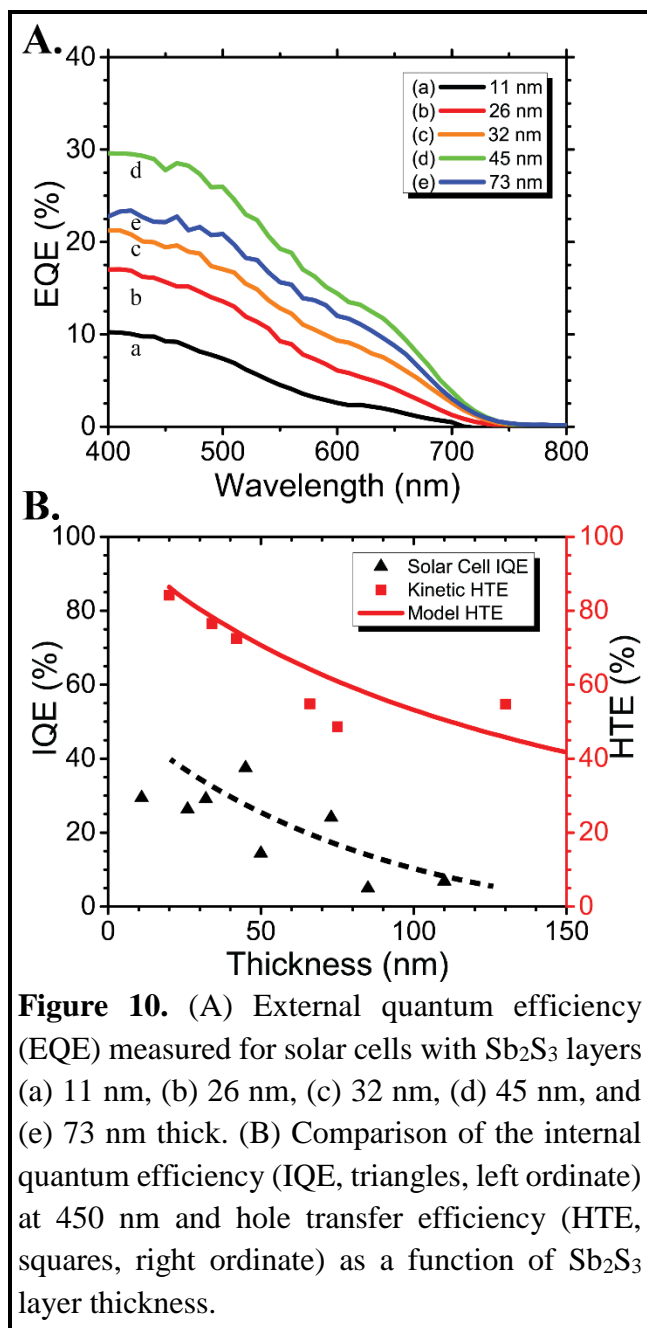


Figure 10. (A) External quantum efficiency (EQE) measured for solar cells with Sb₂S₃ layers (a) 11 nm, (b) 26 nm, (c) 32 nm, (d) 45 nm, and (e) 73 nm thick. (B) Comparison of the internal quantum efficiency (IQE, triangles, left ordinate) at 450 nm and hole transfer efficiency (HTE, squares, right ordinate) as a function of Sb₂S₃ layer thickness.

the hole transfer dynamics, including the hole transfer rate, is adequately described for all of these Sb₂S₃/CuSCN films by an effective hole diffusion coefficient and interfacial hole transfer coefficient. From this it was shown, by calculation of the hole transfer Biot number (λ), that both diffusion and interfacial transfer are important in dictating the overall hole transfer rate in this system ($\lambda \sim 1$). However, high efficiency Sb₂S₃ photovoltaics utilize mesoporous TiO₂ substrates with high surface roughness so that the Sb₂S₃ layer is generally less than 20 nm.¹⁷ For a 20 nm Sb₂S₃ film the hole transfer Biot number is estimated as $\lambda = 0.10 \pm 0.01$. This low Biot number implies that interfacial transfer is the rate limiting step for hole transfer in these devices.

$$HTE = k_{ht} / (\langle \tau \rangle_{Sb_2S_3}^{-1} + k_{ht}) \quad (23)$$

where k_{ht} is the rate of hole transfer, and $\langle \tau \rangle_{Sb_2S_3}$ is the average lifetime of the S^{-•} induced absorption without CuSCN.

These results show that solar cell IQE closely follows the HTE calculated by transient absorption spectroscopy. From this, we conclude that HTE is a very important contributing factor to the efficiency of charge extraction in TiO₂/Sb₂S₃/CuSCN photovoltaics. However, IQE was lower in all cases than HTE for similar Sb₂S₃ thickness, implying that other factors such as back electron transfer, inefficient charge collection, and inefficient electron extraction also contribute to the lower IQE.

Conclusions

This study comprehensively investigates the role and mechanism of hole transfer in solid-state Sb₂S₃ solar cells. Due to diffusion of holes in the Sb₂S₃ films, the observed hole transfer rate, as measured by femtosecond transient absorption spectroscopy, decreased over an order of magnitude from $1.15 \pm 0.6 \times 10^9 \text{ s}^{-1}$ for 20 nm thick Sb₂S₃ films to $2.6 \pm 0.8 \times 10^8 \text{ s}^{-1}$ for 130 nm thick films. We show that the

Confirmation of the role of interfacial transfer is seen by employing a simplified model that neglects interfacial hole transfer limitations through absorbing boundary conditions. This simplified model is unable to adequately fit the time-resolved kinetic data for Sb_2S_3 and predicts an increasing diffusion constant with increasing Sb_2S_3 thickness. In spite of this, it is shown that this simplified model provides an accurate prediction of productive absorber thickness, 50 nm, from the apparent diffusion length, L_{DA} , by combining diffusion, interfacial transfer, and recombination effects into one parameter. This result was confirmed through the construction of planar photovoltaics in which the peak short-circuit current was observed with a 45 nm Sb_2S_3 layer. In addition, planar Sb_2S_3 photovoltaics demonstrate that hole transfer is an important limiting parameter in photovoltaic performance.

In summary, it is shown that interfacial hole transfer, not mobility, is the most important parameter limiting the productive absorber thickness and hole transfer rate in high efficiency Sb_2S_3 photovoltaics. In addition, we provide an estimate of hole mobility ($\mu = 2.6 \pm 1.9 \text{ cm}^2 \text{ V}^{-1} \text{ s}^{-1}$) in Sb_2S_3 under experimental conditions closely resembling those of an actual solar cell. Understanding the mechanism by which hole transfer is controlled is important for the further optimization of materials and interfaces in these photovoltaics. Therefore, it is crucial to take into account transfer across the donor/acceptor interface to obtain an accurate picture of the processes involved.

Experimental Methods

Materials

Antimony chloride (SbCl_3 , Alfa Aesar, 99%), copper(I) thiocyanate (CuSCN , Strem Chemicals, 99%), di-n-propyl sulfide ($\text{C}_6\text{H}_{14}\text{S}$, Alfa Aesar, 98%), potassium thiocyanate (KSCN , Aldrich, 99%), sodium thiosulfate pentahydrate ($\text{Na}_2\text{S}_2\text{O}_3 \cdot 5\text{H}_2\text{O}$, Alfa Aesar, 99%), titanium diisopropoxide bis(acetylacetonate) ($[(\text{CH}_3)_2\text{CHO}]_2\text{Ti}(\text{C}_6\text{H}_7\text{O}_2)_2$, Sigma Aldrich, 75 wt.% in isopropanol), and zinc powder (median 6 – 9 μm , Alfa Aesar, 97.5%) were used without further purification.

Preparation of Sb_2S_3 Films for Transient Absorption Spectroscopy.

Glass microscope slides (2 cm x 0.7 cm) were cleaned in a detergent solution in an ultrasonic bath for 15 min, rinsed with water and ethanol, and heated at 500 °C for 5 min. A compact TiO_2 layer (~150 nm) was deposited by spray pyrolysis from a 0.2 M solution of titanium diisopropoxide bis(acetylacetonate) in ethanol at 400 °C.⁴⁹ Deposition of Sb_2S_3 was carried out by chemical bath deposition (CBD) at 7 °C for 20 – 90 min.²⁴ The slides were removed, rinsed with water, and then dried with a soft stream of air. The as-deposited films were annealed under nitrogen for 20 min at 300 °C until they turned to dark brown,

crystalline, stibnite. After annealing, films were stored in dry air until further characterization. Following characterization of the $\text{TiO}_2/\text{Sb}_2\text{S}_3$ films, a CuSCN layer was applied to be able to compare identical Sb_2S_3 films with and without CuSCN. Before CuSCN application, the Sb_2S_3 films were immersed in a 0.5 M aqueous KSCN solution for 5 min. The films were removed and excess KSCN was wicked away. $10\mu\text{L}/\text{cm}^2$ of 0.05 M CuSCN solution in di-n-propyl sulfide was deposited at $15\mu\text{L}/\text{min}$ while the deposition needle was moved over the film at $1\text{ mm}/\text{s}$. The substrate was placed on a hotplate at $80\text{ }^\circ\text{C}$ and deposition was carried out using a homemade deposition apparatus similar to that reported by O'Regan *et al.*⁵⁰ The completed films were then stored in dry air until further characterization.

Fabrication of Solar Cells

A portion of the fluorine doped tin oxide (FTO) glass substrates (Pilkington Glass, TEC-7, 2 mm thickness) were masked and a thin layer of Zn powder was applied on the unmasked section. Concentrated HCl was dripped over the Zn powder and allowed to sit for approximately 10 sec to completely etch away the FTO layer before washing with H_2O . The etched FTO substrates (2 cm x 1.5 cm) were then cleaned and TiO_2 , Sb_2S_3 , were deposited as described above for the Sb_2S_3 films used for transient absorption spectroscopy. $40\mu\text{L}/\text{cm}^2$ of 0.05 M CuSCN solution was deposited at $20\mu\text{L}/\text{min}$ in the same way as for transient absorption films. To complete the solar cell, an Au contact (100 nm) was evaporated on the CuSCN to form the back electrical contact. The solar cell active area was masked (typically $\sim 0.10\text{ cm}^2$) and the precise active area was determined using *ImageJ* image analysis software.⁵¹ Complete solar cells were illuminated at open-circuit under $100\text{ mW}/\text{cm}^2$ AM 1.5G irradiation for 2 h before measurement.¹⁶

Optical, and Photovoltaic Characterization.

UV-visible absorption spectra were recorded using a Varian Cary 50 Bio spectrophotometer. A 300 W Xe lamp with an AM 1.5G filter was used to irradiate the solar cells at $100\text{ mW}/\text{cm}^2$ and short-circuit current measurements were carried out using a Princeton Applied Research 2273 (PARstat) potentiostat. Incident photo to carrier efficiencies (IPCE) were measured using a Newport Oriel QE/IPCE measurement kit with a silicon photodiode reference detector.

Femtosecond Transient Absorption.

Femtosecond transient absorption measurements of $\text{TiO}_2/\text{Sb}_2\text{S}_3$ and $\text{TiO}_2/\text{Sb}_2\text{S}_3/\text{CuSCN}$ films were conducted using a Clark MXR 2010 (775 nm, 1 mJ/pulse, fwhm pulse width = 130 fs, 1 kHz repetition rate) and an Ultrafast Systems (Helios) UV-visible detection system. The fundamental laser output was split into pump (95%) and probe (5%) beams. The pump beam was directed through a second harmonic frequency doubler to produce the 387 nm pump beam and the probe beam passed through an optical delay

rail and was focused on a Ti:sapphire crystal to produce a white light continuum. The pump was attenuated at 40 $\mu\text{J}/\text{pulse}$ and the optical delay stage provided a probe time window of 1.6 nm with a step resolution of 7 fs. Kinetic traces were assembled at the appropriate wavelengths from the time-resolved spectral data. All films studied were placed in evacuated quartz cells for measurement.

Acknowledgements

The research described herein was supported by the Division of Chemical Sciences, Geosciences, and Biosciences, Office of Basic Energy Sciences of the U.S. Department of Energy through award DE-FC02-04ER15533. This is contribution number NDRL No. 4993 from the Notre Dame Radiation Laboratory.

Supporting Information

Included are control femtosecond transient absorption experiments using TiO_2 , CuSCN, and $\text{TiO}_2/\text{CuSCN}$ films, and a complete derivation of hole transfer kinetic model along with necessary assumptions.

References

1. P. V. Kamat, *J. Phys. Chem. Lett.*, 2013, **4**, 908–918.
2. P. V. Kamat, *J. Phys. Chem. C*, 2007, **111**, 2834–2860.
3. N. Park, *J. Phys. Chem. Lett.*, 2013, **4**, 2423–2429.
4. M. Grätzel, *Nature*, 2001, **414**, 338–344.
5. G. Hodes and D. Cahen, *Acc. Chem. Res.*, 2012, **45**, 705–713.
6. B. Li, L. Wang, B. Kang, P. Wang, and Y. Qiu, *Sol. Energy Mater. Sol. Cells*, 2006, **90**, 549–573.
7. M. Grätzel, *Comptes Rendus Chim.*, 2006, **9**, 578–583.
8. P. P. Boix, G. Larramona, A. Jacob, B. Delatouche, I. Mora-Seró, and J. Bisquert, *J. Phys. Chem. C*, 2012, **116**, 1579–1587.
9. C. Lévy-Clément, R. Tena-Zaera, M. A. Ryan, A. Katty, and G. Hodes, *Adv. Mater.*, 2005, **17**, 1512–1515.

10. I. Mora-Seró, S. Giménez, F. Fabregat-Santiago, E. Azaceta, R. Tena-Zaera, and J. Bisquert, *Phys. Chem. Chem. Phys.*, 2011, **13**, 7162–7169.
11. Y. Zou, D. Li, X. Sheng, L. Wang, and D. Yang, *Sol. Energy*, 2012, **86**, 1359–1365.
12. G. Larramona, C. Choné, A. Jacob, D. Sakakura, B. Delatouche, D. Péré, X. Cieren, M. Nagino, and R. Bayón, *Chem. Mater.*, 2006, **18**, 1688–1696.
13. A. Belaidi, T. Dittrich, D. Kieven, J. Tornow, K. Schwarzburg, and M. Lux-Steiner, *Phys. Status Solidi - Rapid Res. Lett.*, 2008, **2**, 172–174.
14. J. A. Chang, S. H. Im, Y. H. Lee, H.-J. Kim, C.-S. Lim, J. H. Heo, and S. Il Seok, *Nano Lett.*, 2012, **12**, 1863–1867.
15. P. P. Boix, Y. H. Lee, F. Fabregat-Santiago, S. H. Im, I. Mora-Sero, J. Bisquert, and S. Il Seok, *ACS Nano*, 2012, **6**, 873–880.
16. S. Nezu, G. Larramona, C. Choné, A. Jacob, B. Delatouche, D. Péré, and C. Moisan, *J. Phys. Chem. C*, 2010, **114**, 6854–6859.
17. Y. Itzhaik, O. Niitsoo, M. Page, and G. Hodes, *J. Phys. Chem. C*, 2009, **113**, 4254–4256.
18. S.-J. Moon, Y. Itzhaik, J.-H. Yum, S. M. Zakeeruddin, G. Hodes, and M. Grätzel, *J. Phys. Chem. Lett.*, 2010, **1**, 1524–1527.
19. K. Tsujimoto, D. Nguyen, S. Ito, H. Nishino, H. Matsuyoshi, A. Konno, G. R. A. Kumara, and K. Tennakone, *J. Phys. Chem. C*, 2012, **116**, 13465–13471.
20. J. A. Chang, J. H. Rhee, S. H. Im, Y. H. Lee, H. Kim, S. Il Seok, M. K. Nazeeruddin, and M. Gratzel, *Nano Lett.*, 2010, **10**, 2609–2612.
21. T. Fujita, K. Kurita, K. Takiyama, and T. Oda, *J. Phys. Soc. Japan*, 1987, **56**, 3734–3739.
22. F. T. F. O'Mahony, T. Lutz, N. Guijarro, R. Gómez, and S. A. Haque, *Energy Environ. Sci.*, 2012, **5**, 9760–9764.
23. N. Bansal, F. T. F. O'Mahony, T. Lutz, and S. A. Haque, *Adv. Energy Mater.*, 2013, **3**, 986–990.
24. J. A. Christians and P. V Kamat, *ACS Nano*, 2013, **7**, 7967–7974.
25. B. Kippelen and J.-L. Brédas, *Energy Environ. Sci.*, 2009, **2**, 251–261.
26. G. Xing, N. Mathews, S. Sun, S. S. Lim, Y. M. Lam, M. Gratzel, S. Mhaisalkar, and T. C. Sum, *Science*, 2013, **342**, 344–347.
27. S. D. Stranks, G. E. Eperon, G. Grancini, C. Menelaou, M. J. P. Alcocer, T. Leijtens, L. M. Herz, a. Petrozza, and H. J. Snaith, *Science*, 2013, **342**, 341–344.
28. A. M. Goodman, *J. Appl. Phys.*, 1961, **32**, 2550–2552.

29. T. Stübinger and W. Brütting, *J. Appl. Phys.*, 2001, **90**, 3632–3641.
30. H. Najafov, B. Lee, Q. Zhou, L. C. Feldman, and V. Podzorov, *Nat. Mater.*, 2010, **9**, 938–943.
31. D. Zhitomirsky, O. Voznyy, S. Hoogland, and E. H. Sargent, *ACS Nano*, 2013, **7**, 5282–5290.
32. A. Huijser, T. J. Savenije, S. C. J. Meskers, M. J. W. Vermeulen, and L. D. A. Siebbeles, *J. Am. Chem. Soc.*, 2008, **130**, 12496–12500.
33. S. N. Clifton, D. M. Huang, W. R. Massey, and T. W. Kee, *J. Phys. Chem. B*, 2013, **117**, 4626–4633.
34. P. E. Shaw, A. Ruseckas, and I. D. W. Samuel, *Adv. Mater.*, 2008, **20**, 3516–3520.
35. J. Burschka, N. Pellet, S.-J. Moon, R. Humphry-Baker, P. Gao, M. K. Nazeeruddin, and M. Grätzel, *Nature*, 2013, **499**, 316–319.
36. M. Liu, M. B. Johnston, and H. J. Snaith, *Nature*, 2013, **501**, 395–398.
37. J. Z. Zhang, *J. Phys. Chem. B*, 2000, **104**, 7239–7253.
38. C. Ghosh and B. P. Varma, *Thin Solid Films*, 1979, **60**, 61–65.
39. A. M. Karguppikar and A. G. Vedeshwar, *Phys. Lett. A*, 1987, **126**, 123–126.
40. D. R. James, Y.-S. Liu, P. De Mayo, and W. R. Ware, *Chem. Phys. Lett.*, 1985, **120**, 460–465.
41. J. Kirkpatrick, P. E. Keivanidis, A. Bruno, F. Ma, S. A. Haque, A. Yarstev, V. Sundstrom, and J. Nelson, *J. Phys. Chem. B*, 2011, **115**, 15174–15180.
42. A. Faghri, Y. Zhang, and J. R. Howell, *Advanced Heat and Mass Transfer*, Global Digital Press, Columbia, MO, 2010.
43. O. Savadogo and K. C. Mandal, *J. Electrochem. Soc.*, 1994, **141**, 2871–2877.
44. D. E. Mears, *Ind. Eng. Chem. Process Des. Dev.*, 1971, **10**, 541–547.
45. Y. Xu and Y. Zhang, *Atmos. Environ.*, 2003, **37**, 2497–2505.
46. D. Bi, L. Yang, G. Boschloo, A. Hagfeldt, and E. M. J. Johansson, *J. Phys. Chem. Lett.*, 2013, **4**, 1532–1536.
47. K. Tvrdy, P. A. Frantsuzov, and P. V. Kamat, *Proc. Natl. Acad. Sci. U. S. A.*, 2011, **108**, 29–34.
48. V. Chakrapani, D. R. Baker, and P. V. Kamat, *J. Am. Chem. Soc.*, 2011, **133**, 9607–9615.
49. L. Kavan and M. Grätzel, *Electrochim. Acta*, 1995, **40**, 643–652.
50. B. C. O'Regan and F. Lenzmann, *J. Phys. Chem. B*, 2004, **108**, 4342–4350.

51. C. A. Schneider, W. S. Rasband, and K. W. Eliceiri, *Nat. Methods*, 2012, **9**, 671–675.